Journal of Applied Polymer Science

Defect minimization and feature control in electrospinning through design of experiments

Matteo Borrotti,[1] Ettore Lanzarone,[1] Fabio Manganini,[1] Simona Ortelli,[2] Antonio Pievatolo,[1] Cinzia Tonetti[3]

[1]CNR-IMATI, Milan, Italy
[2]CNR-ISTEC, Faenza, Italy
[3]CNR-ISMAC, Biella, Italy
Correspondence to: E. Lanzarone (E-mail: ettore.lanzarone@cnr.it)

ABSTRACT: Electrospinning is affected by high variability, and an accurate setting of process parameters is fundamental for producing high quality nanofibers. This work aims at determining the optimal values of the main process parameters (polymer concentration, polymer feed rate, and voltage) as a function of the environmental factors (temperature and humidity), in order to obtain nanofibrous materials within a specific range of fiber diameter and porosity, and at the same time to minimize production defects. The response surfaces of diameter, porosity, and defects are first determined with a central composite design. These surfaces are then employed as an input for the optimization problem: diameter and porosity surfaces are used to constrain an admissible region, where the minimum of the defect surface is searched. The approach is tested on a prototype electrospinning machine. The estimated response surfaces capture the variability of the process with respect to both production parameters and environmental factors, and are capable of getting the optimal values of the process parameters. © 2017 Wiley Periodicals, Inc. J. Appl. Polym. Sci. **2017**, *134*, 44740.

KEYWORDS: defect minimization; design of experiments; electrospinning; nanofibrous materials; production optimization

Received 15 April 2016; accepted 3 November 2016
DOI: 10.1002/app.44740

INTRODUCTION

Electrospinning is the most promising and versatile process for producing nanofibrous materials[1,2]; it directly produces nanostructured materials, without self-assembly, in the form of nonwoven fibers. Electrospun scaffolds show high surface-to-volume ratios, controlled porosity and flexibility in conforming to a wide variety of sizes and shapes.[1,3]

The structure of the produced material is influenced by several variables, which can be divided into *process factors* (e.g., solution feed rate, applied voltage and polymer concentration) and *environmental conditions* (e.g., temperature and relative humidity). Moreover, depending on the value assumed by process and environmental variables, the produced nanofibrous materials may exhibit structural defects (beads or flattened areas) and non-uniform distributions (alternation of big pores and dense material, and sparse fiber diameter distribution), which may alter the properties of the nanofibrous material,[4,5] e.g., mechanical[6] and filtration[7,8] properties. Thus, the main challenge of electrospinning is to produce fibers with the desired characteristics and at the same time to reduce defects and non-uniform distributions. This problem, still not completely solved, limits the industrial applicability of electrospinning on a large scale.[9]

In this article, an optimization framework is developed to improve the quality of the nanofibrous material produced by electrospinning: the optimal values of process factors are determined both to minimize defects and meet given constraints on fiber characteristics, also considering environmental conditions.

The optimization of the production process requires the response functions that relate the characteristics and defects of the produced material to the process and environmental variables. An approach based on the physical laws that underlie the process is impracticable, due to the presence of several phenomena and to a high complexity at reduced scale. A more effective approach is to determine fair cause-effect surfaces that match the experimental observations. For this purpose, a statistical design of experiments (DOE) framework is considered in this work. The response surface methodology (RSM) is adopted, as it is commonly employed when the objective of the analysis is to optimize the system response, i.e., the values of one or more response variables.[10]

This article was published online on 20 January 2017. An error was subsequently identified. This notice is included in the online and print versions to indicate that both have been corrected 27 January 2017.

In the literature, DOE has proved to be a powerful instrument to study the correlation between fiber diameter and process factors.[11,12] However, experimenters limited their analyses to factors that exhibit an influence only on one process output (e.g., the fiber diameter or the defect ratio) and built up regression models to inspect only these specific relationships.[12–14] In this work a more flexible tool is proposed, which includes three response variables related to both the defects and the structural characteristics of the fibers, namely: (1) the defect ratio; (2) the fiber diameter; and (3) the size of pores. In particular, exploiting the RSM idea, a 2^3 central composite design based on 20 runs is adopted.[10] All data are obtained from scanning electron microscope (SEM) images of electrospun nanofibrous materials, which are processed by automated computer algorithms to obtain the values of the response variables.

The regression models are combined into a constrained optimization problem: diameter and pore response surfaces are used to identify an admissible region, where the minimum of the defect surface is searched. The process parameters obtained in this way yield a fiber mat with the desired morphological properties (diameter and porosity falling within a prescribed range of values) and ensure that the defects are as few as possible. The proposed model also takes into account the effect of uncontrolled environmental factors, i.e., room temperature and relative humidity, which are known to affect the fiber mat structure.[15,16]

This approach has been applied to polyethylene oxide (PEO) on a prototype electrospinning apparatus; however, it can be easily extended to other applications, because the framework always remains the same, whereas the chosen variables (process factors, environmental variables, and output parameters) and the results depend on the specific material and electrospinning machine pair. In particular, the response surfaces must be recomputed every time a new material is spun, a new electrospinning system is adopted, or a new process variable is included (see Ref. 17 for other process variables).

EXPERIMENTAL

Electrospun Material and Electrospinning Apparatus

PEO with average molecular weight $M_w = 4 \times 10^5$ g/mol (purchased from Sigma-Aldrich, MO) was electrospun. It was dissolved in deionized water at given concentrations, and the obtained solutions were kept under magnetic stirring for 18 h, at 100 rpm and temperature of 20 ± 2 °C, in order to ensure complete PEO dissolution in water. All solutions were then stored at the same temperature before electrospinning.

PEO solutions were electrospun into nanofibers with the typical electrospinning setup. A plastic syringe was filled with about 4 mL of solution, and the solution was pushed at a fixed flow rate by a high-precision syringe pump (KDS200, KD Scientific Inc., MA) through a stainless steel tip with an internal diameter of 0.2 mm connected to the syringe. The tip was electrically connected to a generator (SL50, Spellman High Voltage Electronics Corp., NY), which supplied voltage. A stainless steel plate of 20 cm × 20 cm was placed in front of the tip, at a distance of 20 cm, as a nanofiber collector; the collector was electrically grounded. During electrospinning, temperature and humidity were recorded with an Escort iLog RH data logger (Eclo, Portugal) every minute. Nanofibers were collected for 20 ± 1 min for each sample; this duration is enough to get a proper electrospun sheet and to derive information about the process.[18–20]

Input and Output Variables

Two types of input variables were considered, i.e., process factors (which can be controlled) and environmental factors (which cannot be directly controlled on the machine and depend on the room where the process takes place). The process factors were: polymer concentration, polymer feed rate and applied voltage. They are among the most significant factors in the electrospinning process, according to both the literature and previous qualitative experiments on the adopted apparatus. They are in fact often used to define the electrospinnability operational range for a specific polymer,[21,22] and they strongly affect nanofiber shape and size. Moreover, they are also relatively easy to control and measure. Concerning the environmental factors, the two most common variables were taken into account, i.e., room temperature and relative humidity.

Summing up, the following factors were included in the analysis (expressed in the reported measurement units):

- x_1: polymer concentration [%];
- x_2: polymer feed rate [mL/s];
- x_3: applied voltage [kV];
- x_4: room temperature [°C];
- x_5: room relative humidity [%].

Practical ranges of the factors are: $5\% < x_1 < 9\%$; $8 \cdot 10^{-5}$ mL/s $< x_2 < 5 \cdot 10^{-4}$mL/s; $15kV < x_3 < 30kV$; $18\,^{\circ}\mathrm{C} < x_4 < 32\,^{\circ}\mathrm{C}$; and $20\% < x_5 < 70\%$. Concentration x_1 is monotonically related to solution viscosity, so there is no need to include the latter among the factors.

The distance between the tip and the plate was fixed at 20 cm, because in some preliminary experiments it was found that the adopted prototype machine did not work properly with other distances in the considered ranges for the other process factors x_1, x_2, and x_3. Moreover, for a future application on a large industrial scale, it will be easier to fix the distance and act on the other factors (a simpler apparatus will be required).

In general, the choice of the most influential factors may depend on the actual experimental conditions and on the apparatus, and other factors can be included.[17] However, the present approach is general and can be adopted for other industrial settings with different process and environmental variables.

As for the output variables, they refer to the morphology and the quality of the produced fiber mat, which are influenced by the above listed factors. Three variables of interest were taken into account:

Defect Ratio y_1 (Expressed in %). Some instabilities may arise during the electrospinning process, leading to the formation of impurities or defects in the fiber mat. Defects can be grouped into two types. (i) beads (polymer droplets): limited portions of

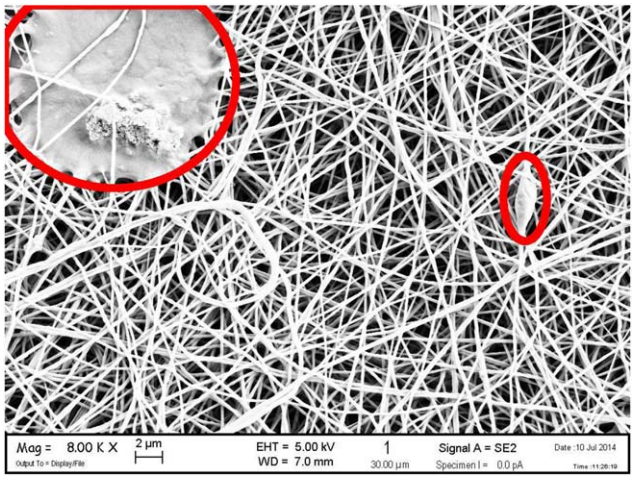

Figure 1. SEM image of an electrospun material, with the two types of defeats circled: a film (on the left) and a bead (on the right). [Color figure can be viewed at wileyonlinelibrary.com]

the fiber showing a significantly larger diameter than the rest of the fiber. They are generated by drops coming off the spinning head, which are deposited on the matrix together with the fibers. (ii) Films (flattened and enlarged polymer depositions): thin layers of material among the fibers. They are related to larger drops that, once deposited on the plate, widen and thin. Then, once the solvent evaporates, a film thinner than the fibers remains in the matrix.

The structural properties of the produced artifact may be severely affected if many defects arise during fiber deposition. Therefore, quantifying defects is highly important. Given an electrospun mat, y_1 is defined as the ratio between the defective surface area A_{def} and the overall surface area of the mat A_{tot}, expressed as a percentage:

$$y_1 = \frac{A_{def}}{A_{tot}} \times 100.$$

Mean Fiber Diameter y_2 (Expressed in nm). The distribution of fiber diameter is of great importance for the structural characteristics of electrospun materials.[23] Understanding how variables affect fiber diameter and its distribution is essential to produce nanofibrous materials with the desired properties. The response y_2 is the average diameter of the fibers in a given electrospun mat.

Mean Pore Size y_3 (Expressed in nm^2). The filtration performance of nanofibrous materials is strongly related to pore size distribution, where pores are the void connected sets in an electrospun mat. The response y_3 is the mean area of the pores. It is also worthwhile to remark that the presence of very large pores with respect to a good reference value is not desired.

The structure of the collected mats was inspected through SEM images. An example of the two types of defects in a SEM image is shown of Figure 1, where beads and films have been circled.

SEM Images

Several SEM images were acquired for each sample using FE-SEM (Carl Zeiss Sigma NTS, Gmbh Öberkochen, Germany). The electrospun samples (4×4 cm) were placed on a metallic support and a thin gold coating (5 nm) was applied on the surface of each sample to ensure a satisfactory electrical conductivity. In order to compare the images, they were all acquired in the same conditions, using the same parameters: magnification = 8000 *X*; extra high tension = 5 kV; working distance = 7 mm; brightness = 45%; contrast = 52%. Response variables were computed from each SEM image through automated computer procedures.

As for the defect ratio y_1, the algorithm proposed in Ref. 24 was adopted. Briefly, the algorithm employs the sparse-approximation technique for representing an image by using a limited number of significant patches, which are collected during a training phase performed on a set of images with no defects. Then, once the training phase is completed, the algorithm detects the patches that do not conform to the training reference distribution (i.e., that correspond to defects) in new SEM images. Thus, A_{def} can be quantified in terms of number of pixels and the defect ratio y_1 is given by A_{def} divided by the total number of pixels. As an example, Figure 2 displays a SEM image both as acquired and with the pixels related to A_{def} marked as spots.

The fast, accurate, easy to implement and totally automated algorithm of Ref. 25 was used for the mean fiber diameter y_2.

Finally, for the mean pore area y_3, the area of the void parts in the fiber mat corresponds to dark areas in the SEM image. Thus, the total area occupied by pores was calculated by simply counting the number of pixels in each black spot, after a thresholding procedure (threshold 20/255).

To increase the reliability of the computed response variables y_1, y_2 and y_3, 50 non-overlapping images were randomly taken from each electrospun sample (a square of 4×4 cm), and the value of each variable was computed as the average across these images.

Central Composite Design

The relationships between each output variable y_i and the input factors x_j were inspected by means of second order regression models, which were fitted to the data obtained from a 2^3 central composite design with six center points and six axial runs.[10]

The two levels for each controlled factor x_1, x_2 and x_3 were obtained from previous experiments,[19,26] to ensure a fairly stable and good quality process output (of course, no value can be imposed on the uncontrollable variables x_4 and x_5).

The design was based on 20 experimental runs, which were performed in a random sequence and on different days to minimize the unwanted effects of unknown and uncontrollable nuisance factors.

For each response variable of interest, a second-order multiple regression model of the following form was fitted:

$$y_i = \beta_0^{(i)} + \sum_j \beta_j^{(i)} x_j + \sum_{j,k:j>k} \beta_{j,k}^{(i)} x_j x_k + \varepsilon_i, \qquad i = 1, 2, 3 \qquad (1)$$

where y_i is the ith response variable, x_j is a process factor or an environmental variable (depending on the index $j = 1, \ldots, 5$),

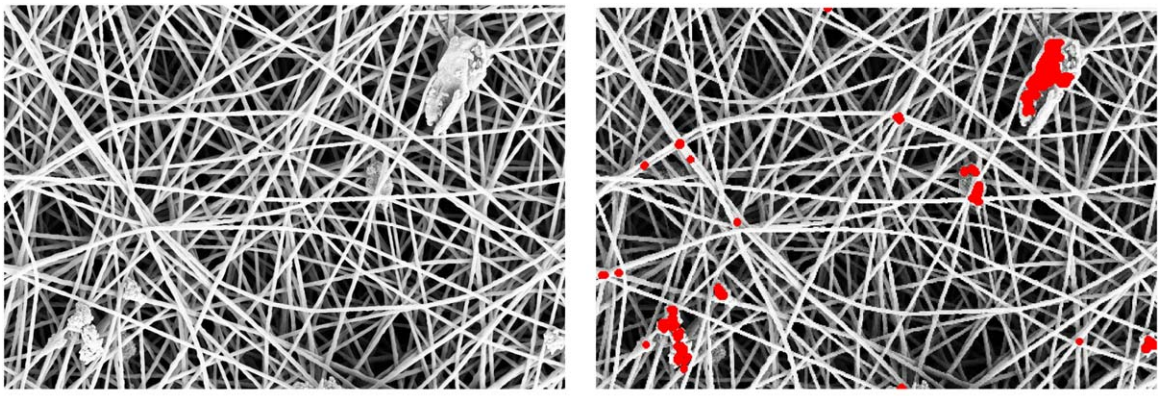

(a) Original (b) Defect detection

Figure 2. Original image of an electrospun mat acquired with the SEM (a); and image with the defects detected and marked as spots (b). [Color figure can be viewed at wileyonlinelibrary.com]

$\beta^{(i)} = \left[\beta_0^{(i)} \quad \beta_1^{(i)} \ldots \beta_5^{(i)} \quad \beta_{1,1}^{(i)} \ldots \beta_{5,4}^{(i)}\right]$ is the vector of the regression coefficients for y_i to be estimated, and ε_i is the model error.

The significant interaction terms included in each model were determined by the Akaike Information Criterion (AIC).[27]

Constrained Optimization for Defect Minimization and Feature Control

The operational conditions for x_1, x_2, and x_3 that ensure an optimal value for y_1, for any fixed value of the uncontrollable variables x_4 and x_5, were obtained from a constrained minimization procedure, in which the response variables y_2 and y_3 were constrained to belong to a selected range of values. In this way, the fiber diameter and the porosity are as desired and the defective areas are kept as small as possible.

It should be noticed that both the fiber characteristics and the defects depend on the same variables; therefore, not all of fiber configurations can be produced with low defect rates, and the material should be produced within a limited range of characteristics to keep defectivity low.

Given an arbitrary pair $(\bar{x}_4, \bar{x}_5)$ of the environmental variables, the triplet of values (x_1^*, x_2^*, x_3^*) that minimize the response y_1 (denoted by y_1^{opt}) and satisfy $y_2 \in I_2$ and $y_3 \in I_3$ is sought, where $I_2 = \left[y_2^{\text{low}}; y_2^{\text{up}}\right]$ and $I_3 = \left[y_3^{\text{low}}; y_3^{\text{up}}\right]$ are the intervals required by the specific application.

The procedure is as follows:

1. Select two domains: $X_c \subset \mathbb{R}^3$ and $X_{nc} \subset \mathbb{R}^2$. The former is associated with the controllable factors (x_1, x_2, x_3); the latter with non-controllable environmental factors (x_4, x_5).
2. Fix an element $(\bar{x}_4, \bar{x}_5) \in X_{nc}$.
3. Predict y_2 and y_3 by evaluating the models in all points $(x_1, x_2, x_3, \bar{x}_4, \bar{x}_5)$ so that $(x_1, x_2, x_3) \in X_c$. Only those points associated with a response that satisfies the constraints $y_2 \in I_2$ and $y_3 \in I_3$ are collected in a subset $\tilde{X}_c \subset X_c$.
4. Predict y_1 by evaluating the model in all points $(x_1, x_2, x_3, \bar{x}_4, \bar{x}_5)$ such that $(x_1, x_2, x_3) \in \tilde{X}_c$ and $y_1 > 0$. The minimum in this set is denoted by y_1^{opt} and the corresponding minimum point is (x_1^*, x_2^*, x_3^*).

By repeating the procedure for every pair $(\bar{x}_4, \bar{x}_5) \in X_{nc}$, it is possible to construct a function $f : X_{\text{nc}} \mapsto y_1^{\text{opt}}$, which is indeed the optimal surface.

Modifications of the set X_{nc}, while I_2 and I_3 remain fixed, only change the domain of the optimal surface, without affecting its values within the domain. It is also possible to extend the set X_{nc}, in order to inspect how the optimal surface behaves on wider areas; however, predictions become unreliable if X_{nc} enlarges too much, as the regression models may become less accurate. In this case, a valid (positive) optimal surface may not exist.

On the contrary, modifications of I_2 and I_3, while keeping X_{nc} fixed, affect the optimal surface as follows: larger/shorter intervals mean less/more restrictive constraints, resulting into a better/worse optimal surface. Notice that, in the presence of short intervals, a valid (positive) optimal surface might not exist. Also notice that there exist maximal ranges for I_2 and I_3 (which are unknown a priori) above which the optimal value will not change anymore.

RESULTS

The estimated regression models are first reported, then the results of some tests conducted to evaluate the behavior of the optimization model are presented. All results were obtained with the considered prototype apparatus.

Regression Models for the Responses

The adopted DOE is shown in Table I. As mentioned, the significant interaction terms were determined with the AIC.[27] Responses y_2 and y_3 turned out to be very correlated, as shown in the scatter plots of Figure 3. This is also in agreement with the literature.[28,29] Hence, a common model for them was adopted by selecting only the terms that are present in both models when fitted to y_2 and y_3 separately, according to the AIC. The coefficients $\beta^{(i)}$ were independently estimated (by least

Table I. Experimental Design

Run	x_1	x_2	x_3	x_4	x_5	y_1	y_2	y_3
1	5.8	0.014	19.9	17.6	34.9	18.9	226.74	46,943
2	7	0.02	23	17.3	35.9	18.7	245.32	59,855
3	8.2	0.014	26.1	17.4	35.6	9.9	265.17	77,158
4	8.2	0.026	19.9	17.8	35.3	15.8	359.42	172,755
5	5.8	0.026	26.1	17.4	35.8	16.2	230.71	57,964
6	7	0.02	23	17.8	35.3	16.5	270.39	76,872
7	8.2	0.026	26.1	19.7	35.0	10.4	280.59	77,080
8	7	0.02	23	19.7	35.7	23.7	243.65	49,395
9	7	0.02	23	19.3	36.3	21.1	261.85	61,017
10	5.8	0.026	19.9	19.0	36.4	18.7	250.33	64,409
11	5.8	0.014	26.1	19.9	35.6	32.5	200.58	33,100
12	8.2	0.014	19.9	19.3	36.8	11.0	285.66	81,720
13	9	0.02	23	19.5	36.9	15.8	311.54	81,899
14	7	0.02	18	20.1	35.7	21.9	258.04	53,108
15	7	0.02	23	20.1	36.4	20.3	253.38	49,627
16	7	0.02	28	19.7	37.3	31.8	223.75	38,590
17	5	0.02	23	19.2	38.3	30.2	210.93	34,195
18	7	0.03	23	19.3	37.8	19.0	289.07	67,148
19	7	0.01	23	19.8	37.2	27.4	227.50	36,828
20	7	0.02	23	19.4	38.3	25.8	247.24	48,630

Independent controlled variables: concentration x_1 (%); feed rate x_2 (mL/min); voltage x_3 (kV). Measured but uncontrolled variables: room temperature x_4 (°C); relative humidity x_5 (%). Response variables: defect ratio y_1 (%); mean fiber diameter y_2 (nm); mean pore area y_3 (nm^2)

squares) for y_2 and y_3 once the terms to be included were selected.

All computations were performed in R,[30] using the package MASS.

The estimated entries of $\beta^{(i)}$ are reported in the model summaries for each i (Tables (II–IV)). Most of them are highly significant for the model; the ones with a lower or null significance have been included because they were retained by the AIC.

The obtained models are statistically significant and there is no violation of model adequacy. Indeed, the residuals show no anomalous behavior (heteroscedasticity, autocorrelation, non-normality). Moreover, the models have high values of the adjusted R^2 (R^2_{adj}) and small values of the residual standard error (RSE), as reported in Table V. Finally, the scatter plots of the response variables predicted by the model ($\hat{y}_i$) versus the experimental values (y_i) are shown in Figure 4; fitted values are homogeneously spread around the bisect line with small dispersion, showing good in-sample predictions.

Constrained Optimization Tests

Three examples of constrained optimization were analyzed to show some outcomes of the proposed optimization approach. Large intervals I_2 and I_3 were fixed in the first one to explore the optimal surface on a wide domain, while narrower intervals were considered in the other examples to represent more realistic and specific production requirements. In all tests, X_{nc}=[17.3,

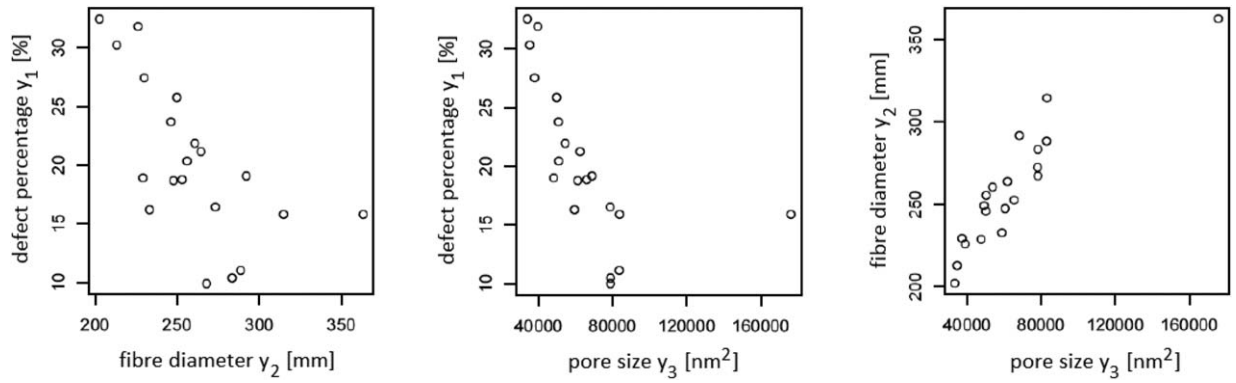

Figure 3. Scatter plots of the response variables: defect ratio y_1 (%), mean fiber diameter y_2 (nm), and mean pore size y_3 (nm^2).

Table II. Model Summary Table for Response Variable y_1 (%)

Term	$\beta^{(1)}$ estimate	Std. error	*t*-value	Pr(>|*t*|)	
Intercept	−2629.6978	903.1568	−2.91	0.017264	*
x_c	−3.6784	0.4292	−8.57	1.27e-05	***
x_v	−163.9678	27.3696	−5.99	0.000205	***
x_p	28.6803	8.3971	3.42	0.007683	**
x_t	134.2391	46.8586	2.87	0.018635	*
x_u	73.2275	25.3558	2.89	0.017943	*
$x_c x_p$	2.6971	0.6531	4.13	0.002561	**
$x_v x_p$	−1.7013	0.5448	−3.12	0.012257	*
$x_v x_u$	4.5868	0.7588	6.05	0.000192	***
$x_p x_t$	−1.6410	0.4441	−3.70	0.004954	**
$x_t x_u$	−3.7084	1.3151	−2.82	0.020055	*

* Significance code (*p* value): 0.05.
** Significance code (*p* value): 0.001.
***Significance code (*p* value): 0

Table III. Model Summary Table for Response Variable y_2 (nm)

Term	$\beta^{(2)}$ estimate	Std. error	*t*-value	Pr(>|*t*|)	
Intercept	16470.419	5101.831	3.228	0.01209	*
x_c	196.146	77.253	2.539	0.03477	*
x_v	280.133	149.755	1.871	0.09831	.
x_p	21.196	2.613	8.111	$3.95 \cdot 10^{-5}$	***
x_t	−841.316	264.734	−3.178	0.01304	*
x_u	−451.159	143.207	−3.150	0.01359	*
$x_c x_v$	−9.509	2.827	−3.364	0.00987	**
$x_c x_u$	−4.484	2.121	−2.114	0.06750	.
$x_v x_p$	−7.558	2.887	−2.618	0.03076	*
$x_v x_t$	2.796	2.534	1.103	0.30199	
$x_v x_u$	−9.653	3.947	−2.446	0.04022	*
$x_t x_u$	23.405	7.429	3.151	0.01359	*

Significance codes as in Table II.

Table IV. Model Summary Table for Response Variable y_3 (nm^2)

Term	$\beta^{(3)}$ estimate	Std. error	*t*-value	Pr(>|*t*|)	
Intercept	14,641,510	5,780,427	2.533	0.03509	*
x_c	327,350	87,529	3.74	0.00571	**
x_v	169,131	169,674	0.997	0.34805	
x_p	14,882	2961	5.026	0.00102	**
x_t	−746,904	299,947	−2.49	0.03751	*
x_u	−402,874	162,255	−2.483	0.03794	*
$x_c x_v$	−15,036	3203	−4.695	0.00155	**
$x_c x_u$	−8417	2404	−3.502	0.00806	**
$x_v x_p$	−10,517	3271	−3.215	0.01234	*
$x_v x_t$	5020	2871	1.748	0.11852	
$x_v x_u$	−7633	4472	−1.707	0.12624	
$x_t x_u$	20,632	8417	2.451	0.03986	*

Significance codes as in Table II.

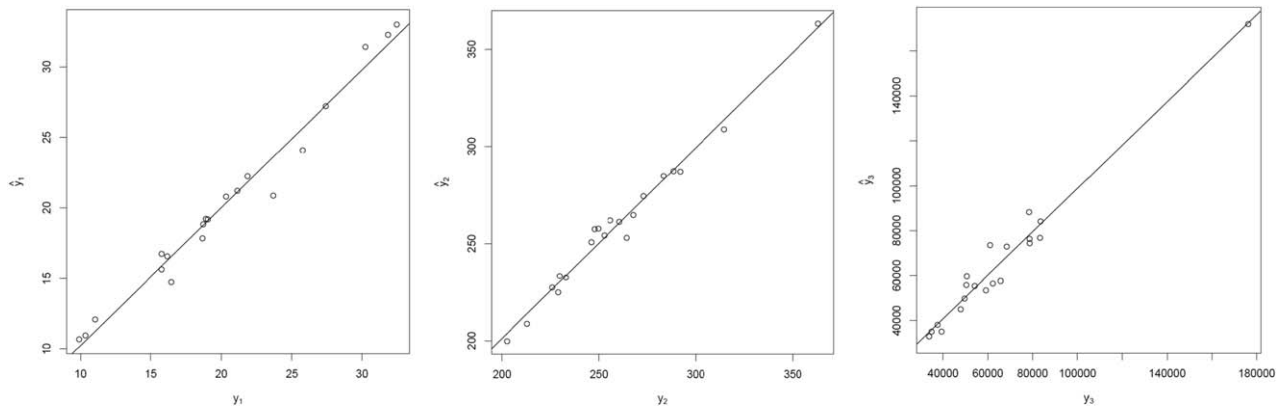

Figure 4. Scatter plots of the fitted ($\hat{y}_i$) versus the experimental (y_i) responses.

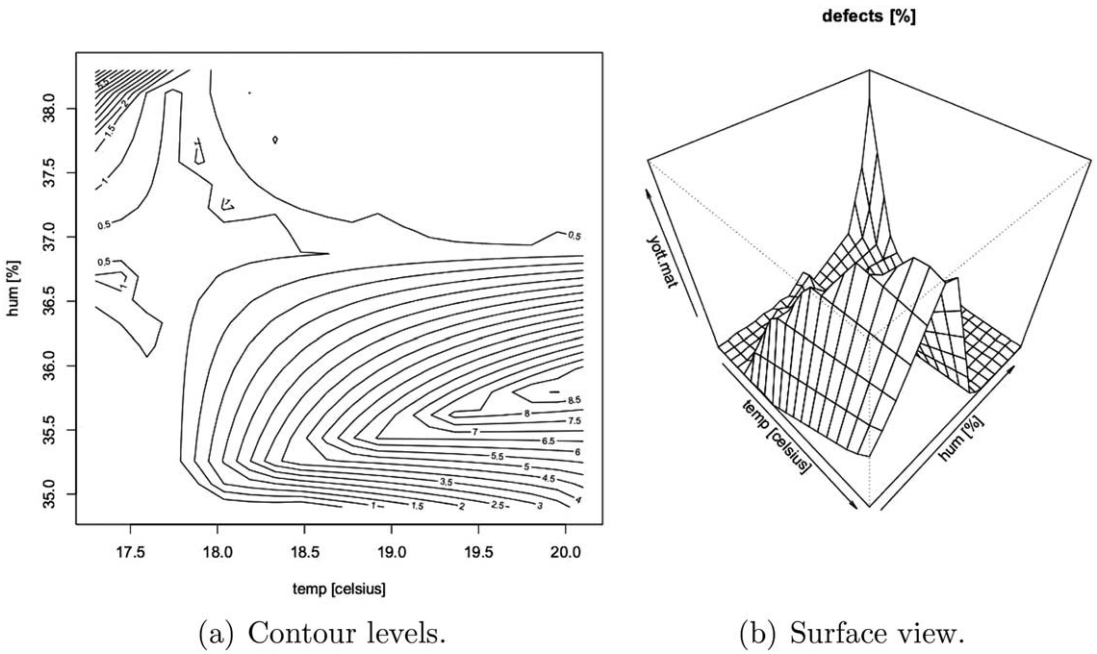

Figure 5. Optimal surface for Test 1.

20.1]×[34.9, 38.3] was kept fixed (i.e., the maximal ranges from the DOE table).

Test 1. Ranges I_2 and I_3 were set equal to the maximal ranges obtained from the computed responses y_2 and y_3 to get a general view of the options at our disposal, i.e., $I_2 = [202, 362]$ and $I_3 = [32{,}400, 176{,}260]$.

Table V. R^2_{adj} and RSE for the Three Regression Models

Model	R^2_{adj}	RSE
y_1	0.9505	1.49
y_2	0.9559	7.769
y_3	0.9184	8803

The optimal surface of y_1, as a function of X_{nc}, is displayed in Figure 5, where every point corresponds to the optimal value given $y_2 \in I_2$ and $y_3 \in I_3$. The model predicts higher defect ratios in two specific regions of the (x_4, x_5) plane. The first region corresponds to low temperature and high humidity, where the optimal surface suddenly increases, while the second region is more spread out than the first one and takes the highest values (defect ratios of about 8.5%) at high temperature and low humidity. These two regions must be avoided in industrial production, as they lead to poor quality nanofibers. On the contrary, production should take place when both temperature and humidity take values that fall outside these regions.

Once the values of x_4 and x_5 are determined (e.g., simply observed for production environments that do not allow an operator to control them), the corresponding optimal values x_1^*,

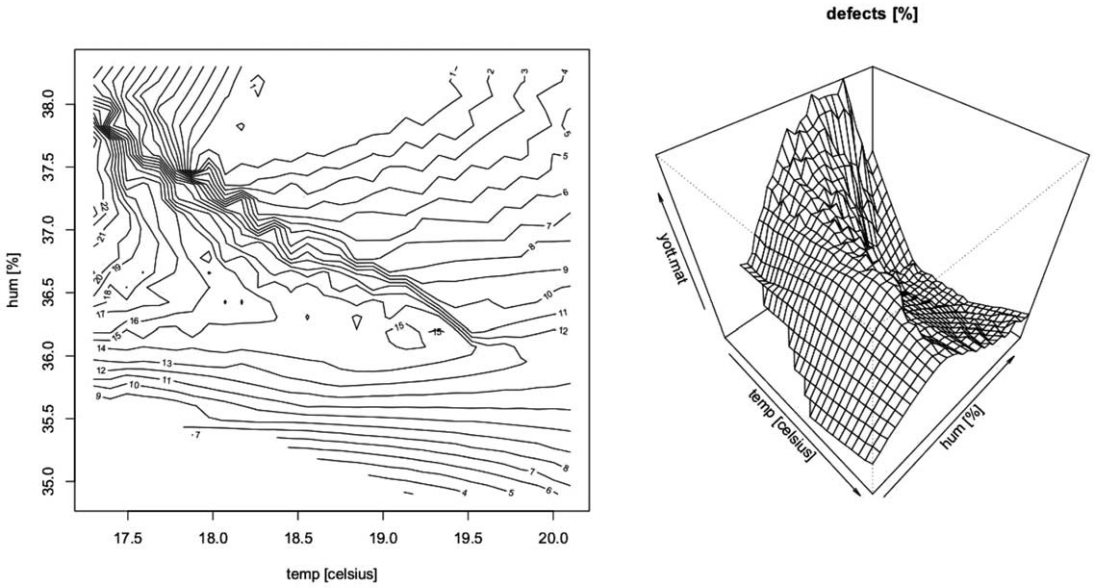

(a) Contour levels. (b) Surface view.

Figure 6. Optimal surface for Test 2.

Table VI. Examples of Optimal Points x_1^*, x_2^*, and x_3^*, Together with the Associated y_1^{opt}, once given $\bar{x}_4$ and $\bar{x}_5$ for Test 1

$\bar{x}_4$	$\bar{x}_5$	x_1^*	x_2^*	x_3^*	y_1^{opt}
17.30	35.61	9.00	0.011	19.05	0.040
18.04	37.04	9.00	0.010	18.00	0.160
19.66	37.58	8.79	0.012	18.52	0.059

x_2^* and x_3^* are derived. To show possible outcomes and to give an idea of the values, Table VI reports the results for three points with low defects in Figure 5. These points are all in the region of the (x_4, x_5) plane where y_1 is low. The associated values of the controlled variables suggest values around $x_1 = 9.00$, $x_2 = 0.011$, and $x_3 = 19.05$ as good production setting.

Test 2. Ranges I_2 and I_3 were restricted to [270, 290] and [60,000, 65,000], respectively.

The optimal surface of y_1 is shown in Figure 6. As expected, in the presence of much narrower intervals than in Test 1, the optimal surface shows higher defects values; here low-defect zones are smaller and the maximum value reaches 23%. Anyway, the general outline of the surface is similar to that of Test 1: the worst production regions are the top-left and bottom-right ones, i.e., low temperature with high humidity, and high temperature with low humidity. Also in this case, once x_4 and

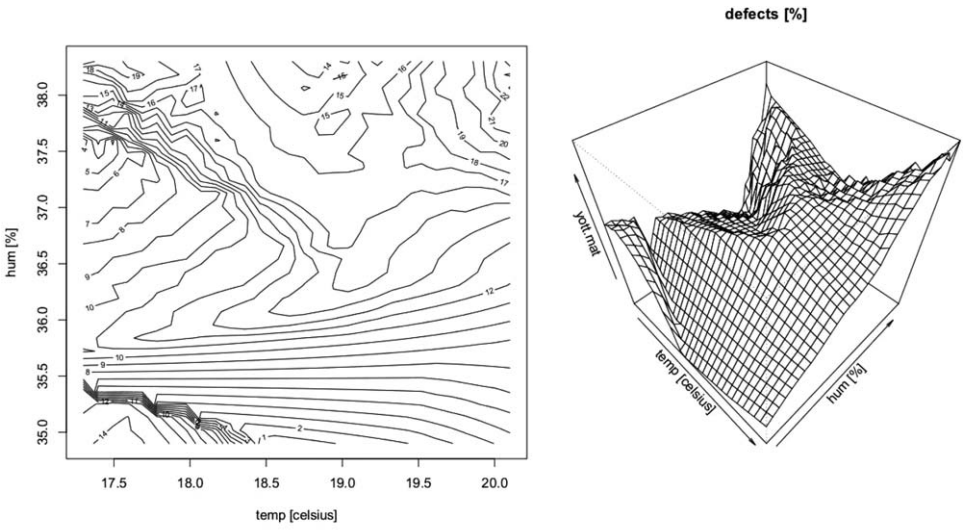

(a) Contour levels. (b) Surface view.

Figure 7. Optimal surface for Test 3.

x_5 are determined, the values of the controllable variables in X_c can be derived.

Test 3. Ranges I_2 and I_3 were restricted to smaller values, i.e., [200, 240] and [40,000, 60,000], respectively.

The optimal surface of y_1 is shown in Figure 7. It significantly differs from both Test 1 and Test 2, as higher defects are predicted and there is no neat zone with remarkably low defect rates. This overall increment of the surface values is in agreement with the relations among the responses y_1, y_2 and y_3. In fact, the selected ranges I_2 and I_3 of this test correspond to high defect values, as shown in the scatter plots of Figure 3.

Hence, this test demonstrates the physical limits of the process, for which it is not possible to obtain any combination of I_2 and I_3 with a good quality in terms of defects. Combinations of I_2 and I_3 that do not respect the correlation between y_2 and y_3 (see Figure 3) are infeasible, but some other feasible conditions are inevitably associated with low quality artifacts.

Finally, the values of the controlled variables in X_c are derived, once x_4 and x_5 are fixed, as shown for Test 1.

Summing up, the selection of the intervals I_2 and I_3 and of the set X_{nc} significantly affect the shape of the optimal surface and the performance of the process. This confirms the importance of the proposed approach, which is able to predict and quantify the impact of the production ranges I_2 and I_3 and of the environmental variables.

CONCLUSIONS

This article proposes a versatile approach to optimize the production of nanofibrous materials by electrospinning, which provides the optimal values of the process factors in order to improve the quality of the produced material. The simultaneous assessment of three response variables (defect ratio, fiber diameter, and mat pore size) achieves the minimization of defects and at the same time it controls the features of the nanofibrous material. Moreover, the dependence of the optimal values upon the environmental conditions allows one to account for external factors that may alter material quality and properties.

With respect to the state of the art, this approach represents an innovative, reliable and practical method to streamline the definition of process parameters and the design of electrospinnable formulations. Indeed, the acquisition of several images coupled with the proposed model provides an efficient control method of both the material and the process.

The procedure adopted is general and can be easily extended to settings other than that presented in this paper, which has been tailored to PEO and to a specific prototype electrospinning apparatus. For instance, a higher number of variables can be included in the set X_c of controllable factors (e.g., the distance between the tip and the plate; see Ref. 17 for a possible list of other factors), and also temperature and humidity can be included in X_c depending on the productive environment. The number of response variables can be also varied. Given the variability among existing electrospinning machines, the approach requires retuning when applied to other cases. The framework always remains the same, but the response surfaces should be recomputed for each new configuration of electrospun material, electrospinning apparatus, or set of variables.

Future work will address the online control of the process because, with the present approach, the optimal production parameters are set at the beginning of the process and do not change afterwards. Corrective actions should be implemented while the electrospinning process runs if some uncontrollable factors change. Even though the approach developed in this paper could still suggest a new optimal point and the way it moves together with the factors, a strategy for a feedback control is also required.

ACKNOWLEDGMENTS

This work has been funded by the Project NanoTWICE (Flagship Project "La Fabbrica del Futuro," call FdF-SP1-T1.2), coordinated by the National Research Council of Italy (CNR) and funded by the Italian Ministry of Education, University and Research (MIUR).

REFERENCES

1. Burger, C.; Hsiao, B. S.; Chu, B. *Annu. Rev. Mater. Res.* **2006**, *36*, 333.
2. Liu, T.; Burger, C.; Chu, B. *Progr. Polym. Sci.* **2003**, *28*, 5.
3. Teo, W. E.; Ramakrishna, S. *Nanotechnology* **2006**, *17*, R89.
4. Deitzel, J. M.; Kleinmeyer, J.; Harris, D.; Beck Tan, N. C. *Polymer* **2001**, *42*, 261.
5. Barua, B.; Saha, M. C. *J. Appl. Polym. Sci.* **2015**, *132*, DOI: 10.1002/app.41918.
6. Chlanda, A.; Rebis, J.; Kijeńska, E.; Wozniak, M. J.; Roznia-towski, K.; Swieszkowski, W.; Kurzydlowski, K. J. *Micron* **2015**, *72*, 1.
7. Yun, K. M.; Hogan Jr., C. J.; Matsubayashi, Y.; Kawabe, M.; Iskandar, F.; Okuyama, K. *Chem. Eng. Sci.* **2007**, *62*, 4751.
8. Bjorge, D.; Daels, N.; De Vrieze, S.; Dejans, P.; Van Camp, T.; Audenaert, W.; Hogie, J.; Westbroek, P.; De Clerck, K.; Van Hulle, S. W. H. *Desalination* **2009**, *249*, 942.
9. Persano, L.; Camposeo, A.; Tekmen, C.; Pisignano, D. *Macromol. Mater. Eng.* **2013**, *298*, 504.
10. Box, G. E. P.; Draper, N. R. Empirical Model-Building and Response Surfaces; Wiley Series in Probability and Statistics; John Wiley & Sons, Inc., USA; **1987**.
11. Coles, S. R.; Jacobs, D. K.; Meredith, J. O.; Barker, G.; Clark, A. J.; Kirwan, K.; Stanger, J.; Tucker, N. *J. Appl. Polym. Sci.* **2010**, *117*, 2251.
12. Cui, W.; Li, X.; Zhou, S.; Weng, J. *J. Appl. Polym. Sci.* **2007**, *103*, 3105.
13. Gu, S. Y.; Ren, J.; Vancso, G. J. *Eur. Polym. J.* **2005**, *41*, 2559.
14. Yördem, O. S.; Papila, M.; Menceloglu, Y. Z. *Mater. Des.* **2008**, *29*, 34.
15. Li, Z.; Wang, C. One-Dimensional Nanostructures – Electrospinning Technique and Unique Nanofibers; Springer: Berlin, Heidelberg, **2013**.

16. De Vrieze, S.; Van Camp, T.; Nelvig, A.; Hagström, B.; Westbroek, P.; De Clerck, K. *J. Mater. Sci.* **2009**, *44*, 1357.
17. Pramanik, S.; Pingguan-Murphy, B.; Abu Osman, N. A. *Sci. Technol. Adv. Mater.* **2012**, *13*, 043002.
18. Aluigi, A.; Vineis, C.; Varesano, A.; Mazzuchetti, G.; Ferrero, F.; Tonin, C. *Eur. Polym. J.* **2008**, *44*, 2465.
19. Rombaldoni, F.; Mahmood, K.; Varesano, A.; Bianchetto Songia, M.; Aluigi, A.; Vineis, C.; Mazzuchetti, G. *Surf. Coat. Technol.* **2013**, *216*, 178.
20. Varesano, A.; Rombaldoni, F.; Tonetti, C.; Di Mauro, S.; Mazzuchetti, G. *J. Appl. Polym. Sci.* **2014**, *131*, DOI: 10.1002/app.39766.
21. Shin, Y. M.; Hohman, M. M.; Brenner, M. P.; Rutledge, G. C. *Polymer* **2001**, *42*, 9955.
22. Zong, X.; Kim, K.; Fang, D.; Ran, S.; Hsiao, B. S.; Chu, B. *Polymer* **2002**, *43*, 4403.
23. Milasius, R.; Malasauskien, J. *Autex Res. J.* **2014**, *14*, 233.
24. Carrera, D.; Manganini, F.; Boracchi, G.; Lanzarone, E. IEEE T Ind Inform **2017**, DOI: 10.1109/TII.2016.2641472.
25. Ziabari, M.; Mottaghitalab, V.; McGovern, S. T.; Haghi, A. K. *Chin. Phys. Lett.* **2008**, *25*, 3071.
26. Dotti, F.; Varesano, A.; Montarsolo, A.; Aluigi, A.; Tonin, C.; Mazzuchetti, G. *J. Ind. Text.* **2007**, *37*, 151.
27. Akaike, H. *IEEE Trans. Autom. Control* **1974**, *19*, 716.
28. Cho, D.; Chen, S.; Jeong, Y.; Joo, Y. L. *Fibers Polym.* **2015**, *16*, 1578.
29. Liu, Y.; Park, M.; Ding, B.; Kim, J.; El-Newehy, M.; Al-Deyab, S. S.; Kim, H. Y. *Fibers Polym.* **2015**, *16*, 629.
30. R Core Team. R: A Language and Environment for Statistical Computing. The R Foundation for Statistical Computing: Vienna, Austria. URL: https://www.R-project.org/